Scientific paper

Synthesis and Characterization of Ordered CuO–CeO_2 Mixed Oxides Using KIT-6 Silica as a Hard Template

Petar Djinović,[a] Urška Kocjan,[a] Jurka Batista[a] and Albin Pintar[a,b,*]

[a] *Laboratory for Catalysis and Chemical Reaction Engineering, National Institute of Chemistry, Hajdrihova 19, P.O. Box 660, SI-1001 Ljubljana, Slovenia*

[b] *Chair of Chemical, Biochemical and Environmental Engineering, Faculty of Chemistry and Chemical Technology, University of Ljubljana, Aškerčeva 5, P.O. Box 537, SI-1001 Ljubljana, Slovenia*

** Corresponding author: E-mail: albin.pintar@ki.si; Tel.: +386-1-47-60-237, fax: +386-1-47-60-300*

Received: 05-02-2009

Abstract

This study focuses on the synthesis of CuO–CeO_2 mixed oxides containing 10, 15 and 20 mol % CuO using hard template method with KIT-6 silica acting as a template. The obtained solids exhibited ordered mesoporous structure, which was identified by N_2 adsorption/desorption and XRD analyses as a negative mold of the KIT-6 silica pore system. The materials were additionally characterized by H_2-TPR/TPD, H_2-TPR/TPO/TPR, selective N_2O chemisorption and NH_3 chemisorption/TPD methods. These methods revealed very high surface area being in the range of 147–166 m^2/g, depending on CuO content and calcination temperature. CuO dispersion values between 28 and 40% were determined by N_2O decomposition with corresponding CuO particle size between 1.3 and 1.9 nm. H_2/TPR-TPO-TPR tests revealed negligible alterations in pore size/volume of calcined solids, indicating good thermal stability of CeO_2 framework under tested conditions. On the other hand, migration and stabilization of surface CuO clusters was detected upon redox cycling, which resulted in noticeable differences in redox behavior. Nevertheless, the ordered and highly porous CuO–CeO_2 materials exhibited superior thermal stability, good redox properties and surface acidity, which render hard template preparation method very useful for the synthesis of ordered mesoporous mixed metal oxides with vast possibilities for future applications in catalysis.

Keywords: Hard template synthesis method, KIT-6 silica, CuO–CeO_2 mixed oxides

1. Introduction

CuO–CeO_2 mixed oxides are very active and selective heterogeneous catalysts for CO and methane oxidation,[1–3] SO_2 reduction with CO,[4,5] NO_x reduction,[6,7] wet oxidation of phenol,[8,9] CO oxidation in excess H_2[10–12] and water-gas shift (WGS) reaction.[13–15] Facile redox interplay between both oxide phases is the key factor of high performances of CuO–CeO_2 catalysts in the above mentioned processes. Enhancement of redox properties has been extensively investigated and explained with strong metal-support interactions occurring between CuO and CeO_2. The occurrence of strong interaction between CeO_2 and supported metal should imply that the interface zone between metal and the support is the most active due to higher lability of the surface oxygen for both noble and transition metals supported on CeO_2.[16–18]

The catalytic activity of modified ceria catalysts greatly depends on particle size, structure distortion and chemical non-stoichiometry (redox properties). In principle, reducing particle size to nano scale and increasing surface area will provide a larger number of more active sites[19] and consequently higher activity in above-mentioned reactions.

Shortcomings of CuO–CeO_2 catalysts are low thermal stability and low specific surface area, compared to non-redox metal oxides, such as SiO_2 or Al_2O_3, which are often successfully used as supports in numerous heterogeneously catalyzed reactions.

One way of overcoming deficiencies of CuO–CeO_2 catalysts is the use of novel preparation methods, which

yield a thermally stable catalyst with a high specific surface area. Hard template synthesis method is reported to yield catalysts with such properties.[20] By using a template with very high porosity and ordered arrays of mesopores, which is impregnated with metal salt solution and leached after precursor mineralization, catalysts with very high surface area can be obtained, which usually cannot be prepared by conventional methods. Furthermore, the internal structure of obtained catalysts is a highly ordered shape-reversed mold of the template pore structure.[21] One such thermally stable and highly porous template is silica. There exist many different mesoporous silicas as suitable templates, but KIT-6 with a cubic *Ia3d* structure, *i.e.* three-dimensionally ordered mesopore arrays and large pore volume, was reported as the most suitable.[19,22] KIT-6 silica exhibits controllable pore size, interconnectivity and high surface area,[21,23] which can be tailored for practical applications by different synthetic pathways.[24] It is of paramount importance to select a template with high thermal stability in order to prevent loss of specific surface area and collapse of its structure during calcination, which would manifest itself in the structure of impregnated catalyst.

Mesoporous CuO–CeO_2 catalysts synthesized following this procedure are composed of nanocrystalline CeO_2 frameworks with high similarities to the cubic *Ia3d* symmetry of the silica template and exhibit remarkable stability in air at temperatures as high as 973 K.[20]

In this work we report on the synthesis and characterization of ordered CuO–CeO_2 mesoporous mixed oxides (with 10, 15 and 20 mol % CuO content) by using a hard template method with KIT-6 silica as template. The obtained CuO–CeO_2 oxides were characterized by various techniques, such as N_2 adsorption/desorption, XRD, H_2-TPR/TPD, H_2-TPR/TPO/TPR, selective N_2O chemisorption and NH_3 chemisorption/TPD, in order to obtain detailed information regarding morphological, redox and surface acidic properties.

2. Experimental

2. 1. Synthesis of KIT-6 silica

High quality KIT-6 material was prepared by adjusting the molar ratio of SiO_2/P123 close to 60[23,25] and the HCl concentration close to 0.75 M.[26] 4 g of Pluronic P123 ($EO_{20}PO_{70}EO_{20}$ poly-(alkylene oxide) based triblock copolymer, MW = 5800, from Aldrich) was added to 144 g of distilled water and 7.5 g of concentrated HCl (37%, from Merck). Afterwards, 4 g of butanol (absolute, p.a., from Merck) was added under stirring and left for 1 hour at 35 °C. Finally, 8.6 g of TEOS ($Si(OC_2H_5)_4$, 99.0% purity, from Fluka) was added and stirred for additional 24 hours at the same temperature.

The obtained gel was transferred into autoclaves and aged at 100 °C for 24 hours under static conditions. This aging/ripening temperature was selected in order to obtain an average pore size of around 8 nm. This was reported as very favorable for impregnation with various metal oxide precursors.[23] Aged slurry was filtered and dried overnight at 100 °C. The dried product was first mixed with 500 ml of ethanol (absolute, p.a., from Riedel-de Haën) and 30 ml of concentrated HCl and stirred at room temperature for 1 h. It was then filtered and washed with 250 ml of distilled water and 150 ml of ethanol. Finally, the product was dried at 60 °C overnight and calcined in air at 550 °C for 5 hours to remove the polymer template.

2. 2. Synthesis of Mesoporous Copper-Cerium Mixed Oxides

Three different CuO–CeO_2 mixed oxide samples were synthesized (with 10, 15 and 20 mol % CuO), which are in the following text referred to as CuCe10, CuCe15 and CuCe20. Appropriate amounts of $Cu(NO_3)_2 \cdot 3H_2O$ (99% purity, from Merck) and $Ce(NO_3)_3 \cdot 6H_2O$ (99% purity, from Aldrich) were dissolved in 25 ml of ethanol (absolute, p.a., from Riedel-de Haën). Amounts of added metal salts were calculated to yield a total metal ion concentration of 0.7 M. Higher concentrations of metal ions are reported to induce formation of bulk metal oxide particles outside the pores of silica.[21] Into 15 ml of this solution, 1 g of KIT-6 was added and stirred at room temperature for 1 hour in order to allow the solution to penetrate and fill the KIT-6 pore system completely. Afterwards the solid was dried overnight at 60 °C. The obtained CuCe15 mixed oxide precursor was heated in a ceramic crucible in an oven at 400 °C for 3 hours to completely decompose the nitrate species. CuCe10 and CuCe20 precursors were calcined at 550 and 450 °C, respectively. The impregnation step was repeated with 10 ml of the ethanol-metal salt mixture for 1 h in order to fill the pores of the silica template with metal salt solution completely. After overnight drying at 60 °C, CuCe15 precursor was again calcined at 400 °C (CuCe10 at 550 °C and CuCe20 at 450 °C) for 3 hours. Optimal calcination temperatures for solids with different CuO loadings, which were determined in our previous work,[27] were employed in this study.

KIT-6 silica template was removed from the resulting solids by leaching twice with 2 M NaOH (Merck) at 50 °C. Traces of NaOH were removed by continuous washing with distilled water and centrifugation until pH value of the slurry reached 7. Finally, the mesoporous CuO–CeO_2 mixed oxide samples were dried overnight at 50 °C.

3. Characterization

Chemical composition of synthesized mixed oxides as well as residual amounts of Si and Na were determined by means of ICP-MS (inductively coupled plasma-mass spectrometry) and ICP-AES (inductively coupled plasma-atomic emission spectroscopy) methods.

Powder X-ray diffraction (XRD) patterns of KIT-6 silica template and CuO–CeO_2 solids were recorded on a PANalytical X'pert PRO diffractometer using Cu Kα radiation (λ = 0.15406 nm). The examined 2θ range was between 10 and 85°, with 0.034° steps and 100 s measuring time at each increment. Low angle X-ray diffraction patterns between 0.5 and 5° were recorded using the same instrument with the angle increasing step of 0.017° and 100 s measuring time at each increment.

N_2 adsorption/desorption measurements were performed using a Micromeritics ASAP 2020 MP/C apparatus. Prior to characterization, the samples were degassed in vacuum (4 μm Hg) at 300 °C. Surface area was determined by the multipoint Brunauer-Emmett-Teller (BET) method, pore volume and pore size distribution were calculated using Barrett-Joyner-Halenda (BJH) method. Average pore size as referred to in the following text is the maximum of pore size distribution.

H_2-TPR, TPO and TPD measurements were performed on a Micromeritics II 2920 catalyst characterization system. For H_2-TPR/TPD and H_2-TPR/TPO/TPR tests, 250 mg of CuCe10, CuCe15 and CuCe20 samples was used. TPR analysis was performed in a 50 ml/min stream of 5% H_2/Ar as a reducing agent. Tested samples were heated from –20 to 400 °C with 5 °C/min ramp during analysis. A liquid nitrogen-isopropyl alcohol cold trap was mounted on exhaust in order to condense water vapor and remove it from the effluent gas mixture, before entering the TCD detector. TPD experiments were performed by heating the reduced sample from –20 to 700 °C in a 50 ml/min Ar flow with a 5 °C/min heating ramp. TPO experiments were carried out by heating the calcined and reduced samples from –20 to 450 °C in a 10% O_2/He gas mixture with a 5 °C/min ramp and recorded with a TCD detector.

CuO phase dispersion was evaluated from pulse N_2O chemisorption after sample calcination, reduction and degassing as reported in our previous publication.[27]

Quantitative analysis of acidic surface sites was carried out by NH_3 chemisorption/TPD analysis. Samples (calcined in synthetic air, reduced in 5% CO/He and degassed at 400 °C in He flow for 3 h) were subjected to pulses of 10% NH_3/He, until surface was saturated. Afterwards, samples were subjected to TPD in a stream of He, while raising the temperature from 90 to 650 °C with a 10 °C/min ramp. The desorbed gasses were identified and quantified using a mass spectrometer (Pfeiffer Vacuum, model Thermostar).

4. Results and Discussion

4. 1. KIT-6 silica Template

4. 1. 1. XRD Characterization

Low angle X-ray diffractogram of synthesized silica template is shown in Figure 1. Peaks belonging to reflections from (211) and (220) crystalline planes, suggest the presence of ordered cubic *Ia3d* structural symmetry[24] and confirm that the synthesized silica precursor is actually KIT-6. High intensity of recorded low angle peaks suggests large dimensions of ordered domains within the investigated sample.

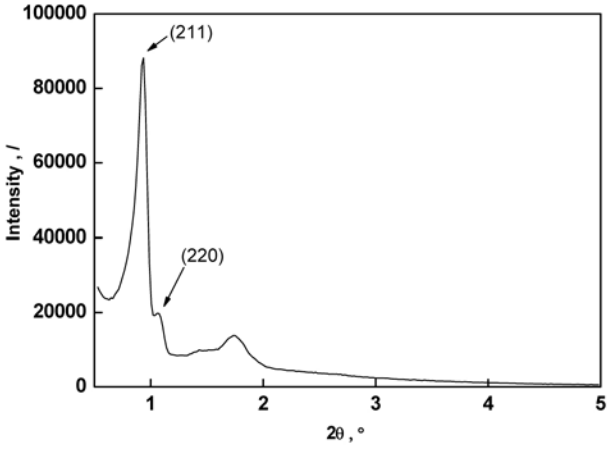

Figure 1. Low angle XRD diffractogram of KIT-6 silica template.

4. 1. 2. N_2 Physisorption and TEM Experiments

N_2 adsorption/desorption isotherm of KIT-6 silica (Figure 2) is of type IV with H1 hysteresis loop, which corresponds to the presence of channel-like pores within the investigated sample. Multipoint BET specific surface area was calculated from the adsorption branch of the isotherm (P/P_o = 0.06–0.30) and reads 600 m^2/g.

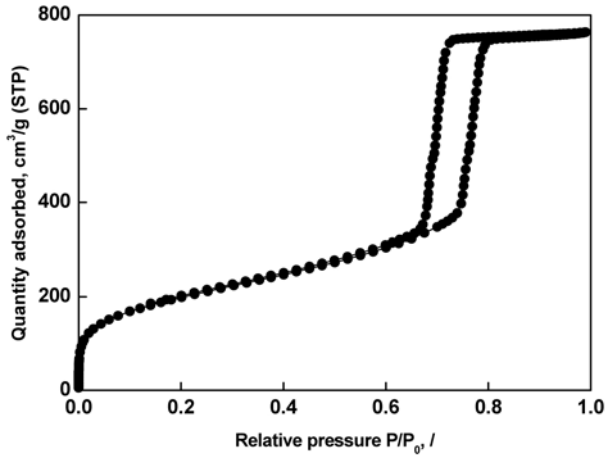

Figure 2. N_2 adsorption/desorption isotherm of the mesoporous KIT-6 silica template.

Pore size distribution of the KIT-6 silica calculated by the Barrett-Joyner-Halenda (BJH) method, is very narrow. A vast majority of pores falls between 5.9 and 8.6 nm, with a maximum (r) at 7.0 nm (Figure 3). Total pore volume in the synthesized KIT-6 silica was calculated to

be 1.43 cm^3/g, which is consistent with the results of other investigations.[19,22]

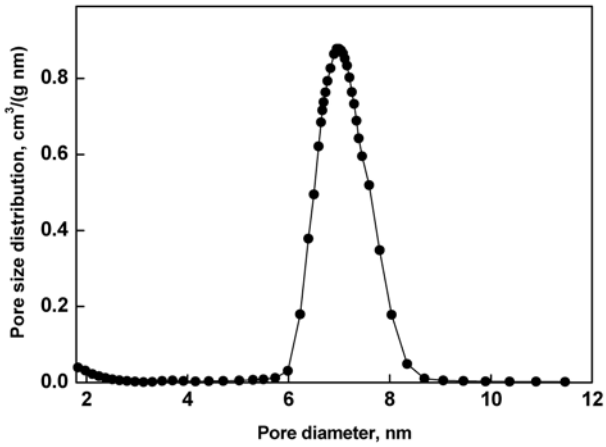

Figure 3. Pore size distribution within the KIT-6 silica template.

A TEM micrograph of synthesized KIT-6 silica template reveals large domains of ordered mesoporous structure, which was also discerned from the low angle XRD diffractogram, presented in Figure 1. Pores of approximately 7 nm in diameter were obtained from carefully inspecting Figure 4, which is in great accordance with the values obtained from N_2 physisorption measurements. Furthermore, KIT-6 pore wall thickness of about 4.5 nm, as determined from Figure 4, resembles closely the value calculated from the XRD diffractograms (approx. 4.7 nm).

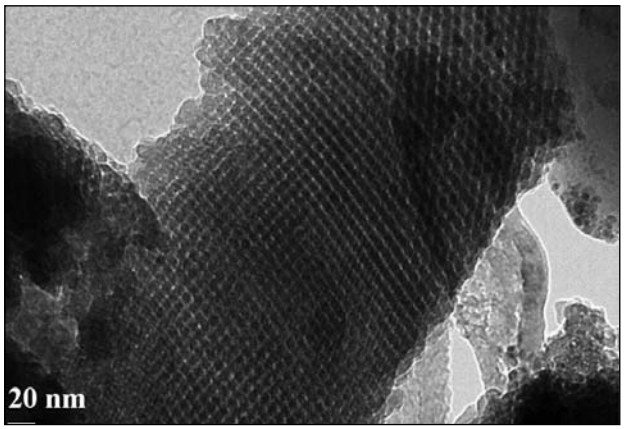

Figure 4. TEM micrograph of KIT-6 silica template.

4. 2. $CuO–CeO_2$ Mixed Oxides

Results of chemical composition analysis of synthesized mixed oxides carried out by ICP-MS and ICP-AES are presented in Table 1. They agree very closely with the nominal values. Minor amounts of Si and traces of Na were detected, despite thorough leaching and washing of CuCe solids. The remaining siliceous residue is very likely encapsulated in the $CuO–CeO_2$ structure and thus could not be removed completely during the leaching process with NaOH.

4. 2. 1. XRD Analyses

The results of XRD analyses are shown in Figure 5. The nanocrystalline nature of the oxide framework can be identified by well-resolved diffraction peaks in the wide angle region of XRD patterns. All recorded peaks were attributed to FCC fluorite CeO_2 phase (PDF data file 03-065-5923). Despite progressively higher CuO loading, no peaks belonging to any ordered copper phase was detected. These observations can be explained by taking into account the fact that CuO particles are extremely small and well dispersed on the CeO_2, and are consequently too small to be detected by XRD analysis.

Very high BET specific surface area of tested samples (Table 1) can accommodate finely dispersed CuO even at relatively high loading of 20 mol %. Average CuO particle size was determined by means of selective N_2O chemisorption experiments, and reads 1.3, 1.9 and 1.7 nm for CuCe10,

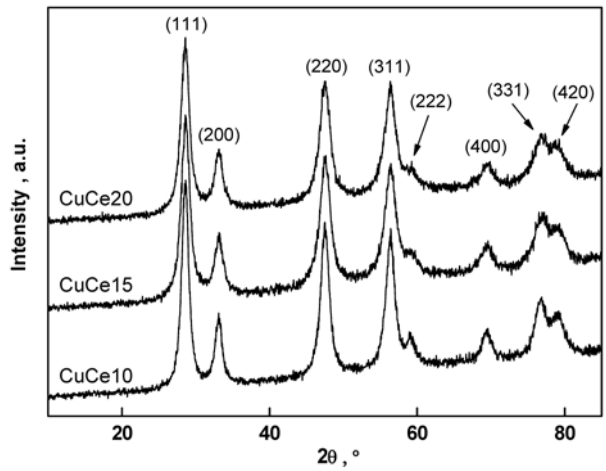

Figure 5. XRD patterns of CuCe10, CuCe15 and CuCe20 samples.

Table 1. Chemical composition, BET surface area and pore volume of calcined CuCe samples before and after reduction.

Sample	CuO, mol %	Si, mol %	Na, ppm	[a]BET surface area, m^2/g	[b]BET surface area, m^2/g	[a]Pore volume, cm^3/g	[b]Pore volume, cm^3/g
CuCe10 550	9.2	1.3	1500	147	139	0.29	0.29
CuCe15 400	14	1.8	100	166	131	0.31	0.28
CuCe20 450	18	1	660	161	147	0.33	0.31

[a] After calcination. [b] After calcination and reduction.

CuCe15 and CuCe20 samples, respectively. Furthermore, no large CuO agglomerates were observed in any of the investigated samples during SEM analysis, which also substantiates the absence of XRD peaks at corresponding CuO 2θ angles.

XRD peak belonging to the reflection from (111) CeO_2 plane was fitted in Origin 7.5 software with Pearson VII function. FWHM (full width at half maximum) was obtained by this procedure and used in the Scherrer's equation to calculate the average CeO_2 crystallite size. It is interesting to note in Table 2 that the calculated average CeO_2 crystallite size corresponds well to the pore size of the parent KIT-6 silica template, presented in Figure 3. This suggests that pore channels of the KIT-6 silica confined the growth of CeO_2 oxide seeds in a limited space and furthermore confirms the replication of mixed metal oxide from the silica template.[22] It is also evident in the case of CuCe10 550 sample that the average CeO_2 crystallite size grows with increasing calcination temperature, as a consequence of sintering, particle agglomeration and growth.

Since no agglomeration of CuO phase was observed in tested materials, we investigated possible formation of a solid solution through the comparison of positions of characteristic peaks belonging to CeO_2. For this purpose, peak positions in Figure 5 were compared to the values of pure CeO_2 from corresponding PDF data file. Negligible difference in peak positions was noticed, regardless of CuO loading and calcination temperature. Similar results were reported previously by Martínez-Arias *et al.*[28] and justified with the fact that substantial differences in Cu^{2+} and Ce^{4+} ion sizes do not allow any noticeable formation of solid solution.

Low angle XRD analyses of CuCe materials were carried out in order to verify any similarity with structural symmetry of the parent KIT-6 template. The presence of small characteristic XRD peaks at 2θ angle of 0.95° is a consequence of reflection from the (211) crystalline plane, which suggests cubic *Ia3d* symmetry also in the CuO –CeO_2 structure (Figure 6), thus reasonably confirming that the prepared CuCe solids are representatives of the KIT-6 pore structure. With increasing CuO loading, the intensity of the characteristic ordered structure reflection and its narrowing implies a substantial increase in the size of ordered domains, indicating positive influence of CuO on the structural order. However, when comparing characteristic low angle reflection peaks of KIT-6 silica to those of CuCe solids, one can see that the latter exhibit much lower intensity and are broader, suggesting that the mixed metal oxide replicas are less ordered than the silica template. The same finding was observed also by Zhu *et al.*[22]

4. 2. 2. N_2 Adsorption/desorption and SEM Analyses

Results of N_2 adsorption/desorption experiments of CuCe solids are presented in Figure 7. The obtained adsorption isotherm is of type IV with H_2 hysteresis loop at a relative pressure between 0.6 and 0.9. The shape of hysteresis loop indicates broader pore size distribution in synthesized CuCe materials, compared to KIT-6 template.

It is obvious that a bimodal pore size distribution exists in the porous structure of synthesized CuCe solids (Figure 8). The first peak corresponds to pores with a diameter of 4.1 nm, which are present in all samples and does not shift with increasing CuO loading. Intensity of the corresponding peak implies that these smaller pores are more abundant in materials with a higher CuO loading. A maximum of the second peak shifts from 6.9 (average pore size of KIT-6 template) to 8.9 nm when CuO content is increased from 10 to 20 mol %.

Bimodal pore size distribution of Co_3O_4 catalysts (maxima at 3.1 and 12.3 nm) prepared by hard template synthesis using KIT-6, was also reported by Jiao *et al.*[29]

Table 2. Morphological, structural, redox and surface acidity results, obtained for CuCe10, CuCe15 and CuCe20 samples.

Sample	Average (111) CeO_2 crystallite size, nm	CuO dispersion, %	Partial CeO_2 reduction, %	TPR, ml/g (STP)	TPO, ml/g (STP)	TPD, ml/g (STP)	Desorbed NH_3, μmol/m^2 (STP)	Desorbed CO_2, μmol/m^2 (STP)	Average CuO particle size, nm
CuCe10 550	7.8	40.4	14.4	30.8	1.97	9.3	1.24	1.78	1.3
CuCe15 400	6.5	28.7	16.1	41.5	2.96	10.7	0.89	2.22	1.9
CuCe20 450	6.6	32.2	24.5	49.8	4.95	9.5	0.92	2.41	1.7

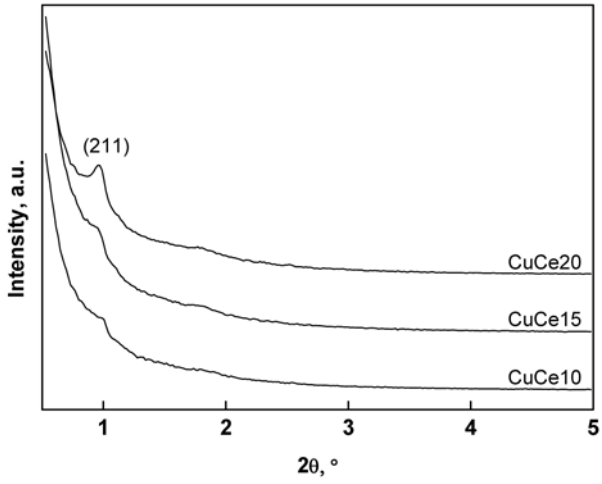

Figure 6. Low angle XRD diffractograms of CuCe10, CuCe15 and CuCe20 samples.

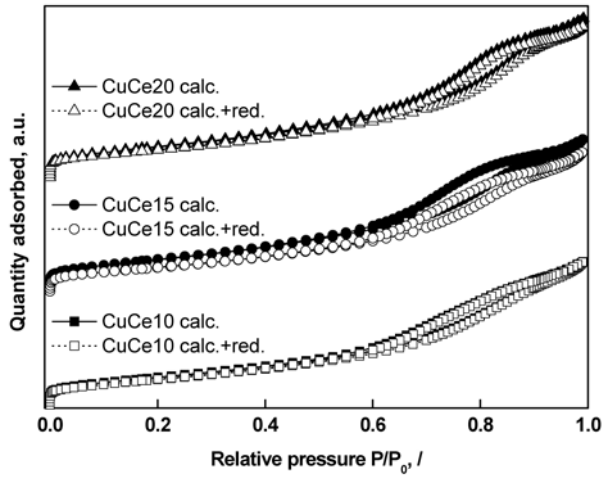

Figure 7. N_2 adsorption/desorption isotherms of calcined CuCe10, CuCe15 and CuCe20 samples before and after reduction. Legend: calc. ≡ after calcination; calc. + red. ≡ after calcination and reduction.

They attributed the former peak to the wall thickness of KIT-6 template, whereas the latter corresponds to the thickness of its wall junctions. When utilizing the hard template synthesis method, the obtained metal oxide solids are a negative mold replica of the KIT-6 skeletal structure; therefore, the pore wall thickness and pore wall junctures should correspond to the pore size of mixed metal oxide after template removal.

In this work, calculation of the KIT-6 wall thickness was adopted from references.[21,29] Low angle KIT-6 (211) peak position and FWHM were obtained by fitting the measured XRD curve with the Pearson VII function. The calculated unit cell parameter (a_0) was 23.5 nm, which is very similar to 22.8 nm value reported elsewhere.[29] The calculated KIT-6 wall thickness (d) was 4.7 nm

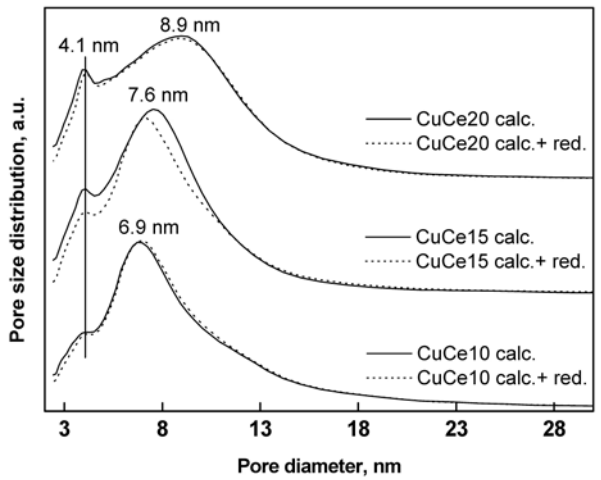

Figure 8. Pore size distribution in CuCe10, CuCe15 and CuCe20 samples before and after reduction. Legend: calc. ≡ after calcination; calc. + red. ≡ after calcination and reduction.

($d = a_0/2–r$), where r is the average pore size of KIT-6 template (Figure 3). The calculated wall thickness is in good agreement with the first peak maximum depicted in Figure 8. Therefore, we can attribute pores centered at around 4.1 nm to be a consequence of template skeletal structure removal. Constant value of this maximum, corresponding to the KIT-6 wall thickness, indicates good stability of the CeO_2 framework and negligible phase migration during leaching and subsequent drying steps. Larger pores observed in the prepared CuCe solids can be attributed to the loading of CuO and CeO_2 precursors around pore wall junctures, and to a certain extent, precipitation outside the KIT-6 template. The second maximum shifts from 6.9 to 8.9 nm with increasing CuO loading, because smaller pores of the KIT-6 template get progressively filled and blocked at higher metal oxide loadings.

BET specific surface area of synthesized CuCe mixed oxides is roughly 3–7 times higher than when CuCe catalysts with the same nominal chemical composition were synthesized by traditional co-precipitation and sol-gel methods.[30] Furthermore, BET surface area was roughly twofold higher compared to CuCe catalysts with 10, 20 and 30% Cu loading, prepared using hard template method[19] and 50% higher compared to CuCe catalysts prepared by the same method.[22] As one can see in Table 1, BET surface area decreases with increasing calcination temperature as a consequence of sintering and particle agglomeration. Increasing CuO content on the other hand does not seem to exhibit any negative effect. Such findings are in contradiction with a common belief, but can be explained quite logically in this case: the average CuO particle size was found to be between 1.3 and 1.9 nm in diameter and pores of the investigated solids are in majority larger than 3 nm, and consequently cannot be blocked with such small CuO clusters.

Some authors report that the ordered mesostructure of CuO–CeO_2 mixed oxides synthesized by means of hard template method, leads to high thermal stability of these materials at temperatures up to 700 °C,[20] compared to regular CuO–CeO_2 materials. To inspect thermal stability under redox conditions, as are often present in CuCe practical applications, BET surface area and pore size/volume of calcined catalysts before and after reduction in H_2 atmosphere at 400 °C for 60 min was measured. As depicted in Table 1, very small difference in total pore volume before and after sample reduction was discerned. BET surface area of CuCe10 and CuCe20 samples decreased for about 10 m^2/g after reduction at elevated temperature and average pore size increased 0.4 nm in size. The largest differences were noticed for CuCe15 sample; in this case, a decrease of BET surface area of about 35 m^2/g was observed. The reason for lower thermal stability and more pronounced morphological alterations of CuCe15 sample originates in low calcination temperature of 400 °C, which is identical to the temperature of subsequent thermal stability test.

4. 2. 3. H_2-TPR/TPD and H_2-TPR/TPO/TPR Tests

Reduction of CuO–CeO_2 mixed oxides consists of several elemental steps, resulting in a TPR profiles (Figure 9), which seemingly comprise of two peaks.[27]

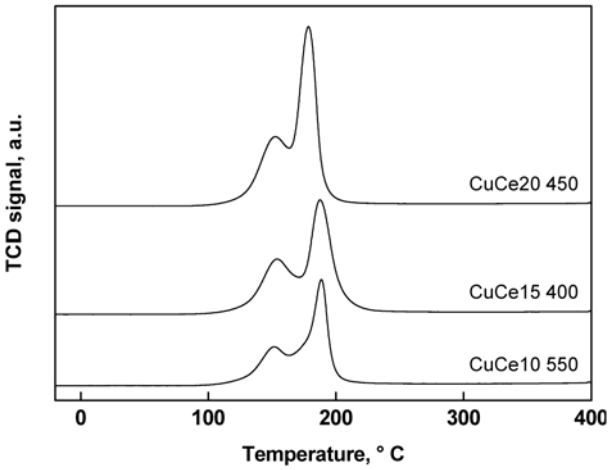

Figure 9. Comparison of H_2-TPR profiles belonging to CuCe10, CuCe15 and CuCe20 samples.

CuO–CeO_2 reduction was in all cases initiated at around 100 °C with the first peak exhibiting a maximum at 155 °C. The second peak maximum was positioned at 180 °C for CuCe20 and at 190 °C for CuCe10 and CuCe15 samples. Complete sample reduction was achieved at temperatures around 225 °C. Reduction process of investigated mixed oxide samples takes place at temperatures, which are much lower than those of individual components,[30] thus proving beneficial effect of strong interactions between both oxide phases.

A detailed analysis of TPR curves revealed a rising quantity of H_2, consumed during sample reduction with increasing CuO loading (Table 2). The amount of H_2 used in the reduction process in all experiments surpassed the quantity needed for complete Cu^{2+} to Cu^0 reduction, indicating considerable extent of CeO_2 support reduction (up to 24.5%) and adsorption on the mixed oxide surface, which does not influence sample reduction. In our previous work we proved that substantial amounts of H_2 can be stored in the CeO_2, which does not contribute to sample reduction and can be quantitatively evaluated by subsequent TPD analysis.[27,30]

As presented in Table 2, similar amounts (9.3, 10.7 and 9.5 ml/g STP) of desorbed H_2 were observed for CuCe10, CuCe15 and CuCe20 samples. This observation alludes that H_2 predominantly adsorbs on CeO_2, the major phase in the investigated system. TPD profiles of CuCe15 and CuCe20 samples consist of three peaks, while an additional fourth peak can be discerned for CuCe10 sample at around 550 °C (Figure 10). A well resolved peak with a maximum at 40 °C, which grows in intensity with increasing CuO loading, is present in all tested materials. The second peak moves progressively towards higher temperatures (maximum occurring at 140, 150 and 170 °C for CuCe10, CuCe15 and CuCe20 samples, respectively). A high-end temperature peak occurs at 430 °C for CuCe10 and CuCe15 solids and shifts to 440 °C for CuCe20, indicating progressively stronger bonding of H_2 for materials with higher CuO loading.

H_2 amounts desorbed during TPD experiments were subtracted from the overall H_2 consumption, yielding the amount of H_2 consumed for CeO_2 reduction. The obtained results are presented in Table 2. With increasing CuO loading the CuO–CeO_2 interface area rises, because a larger amount of CuO is dispersed on the CeO_2 surface. Electronic interactions between the two well dispersed phases facilitate enhanced oxygen mobility within the oxygen sublattice of CeO_2 and thus enhance its reducibility.[18] Partial CeO_2 reduction in the investigated samples was calculated to be 14.4% for CuCe10, 16.1% for CuCe15 and 24.5% for CuCe20, respectively. Greater CuO–CeO_2 interface area in mixed oxides with a higher CuO content seems not only to influence the extent of CeO_2 reduction, but also enables their reduction at lower temperatures, since TPR process is initiated at continuously lower temperature, as CuO content is increased. To conclude, extensive CeO_2 reducibility is of crucial importance to facilitate sufficient activity of CuO–CeO_2 materials in a variety of catalytic processes, including WGS reaction.[27]

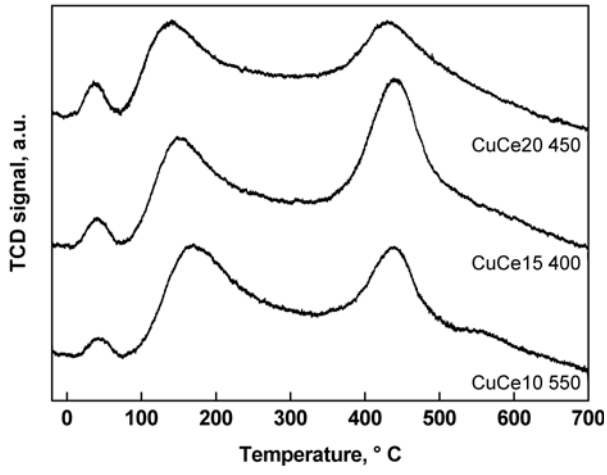

Figure 10. Comparison of TPD profiles belonging to CuCe10, CuCe15 and CuCe20 samples.

By means of N_2 physisorption, no significant alterations of pore size/volume were revealed (see Figures 7, 8 and Table 1) before and after H_2 reduction of calcined samples. As one can further see in Table 1, treatment in H_2 atmosphere (TPR analysis) resulted in small decrease of BET surface area of these solids. These findings indicate

fairly good thermal stability of the CuO–CeO_2 skeletal structure under tested conditions.

More information on the behavior of CuCe solids was obtained by performing H_2-TPR/TPO/TPR cycling. The results are depicted in Figure 11.

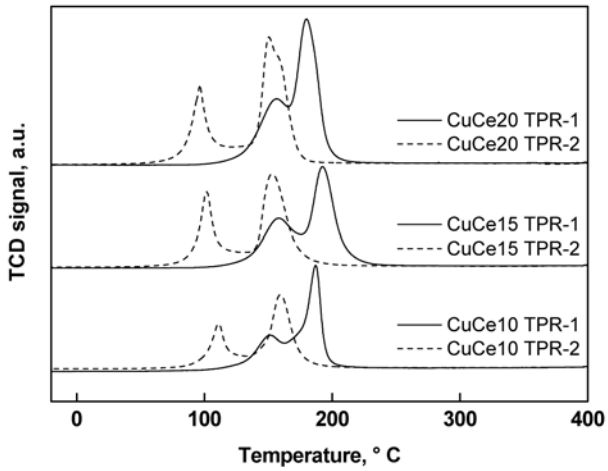

Figure 11. Comparison of TPR-1 and TPR-2 profiles of CuCe10, CuCe15 and CuCe20 samples.

Compared to TPR-1 runs, TPR-2 profiles were for all tested materials shifted toward lower temperatures, indicating easier sample reduction after the first TPR/TPO cycle. These shifts were more pronounced for CuCe15 and CuCe20 samples; for example, lower temperature peak maximum moved for approximately 60 °C, whereas for CuCe10 sample, this shift was about 40 °C. Migration of the higher temperature peak maximum was in all cases less pronounced (30 °C for CuCe10 and CuCe20 solids and 40 °C for CuCe15 samples, respectively). As a result of peak shifting further apart, better separation of particular TPR-2 peaks within each TPR profile was obtained. When comparing corresponding TPR-1 and TPR-2 profiles, the intensity of high temperature peak decreased while the low temperature peak was narrower and increased in intensity. The observed changes of TPR profiles within a TPR/TPO/TPR cycle suggest significant modifications in the nature of reducible species in the investigated samples as a consequence of first TPR/TPO cycle. Very similar observations regarding TPR/TPO/TPR cycling were reported by Caputo *et al.*[31] and attributed to the redistribution of CuO clusters during reduction/oxidation process and their stabilization in lower energy sites. Because the extent of modifications of redox properties of investigated materials was in our case more pronounced for solids with a higher CuO loading, the changes are probably induced by migration of surface CuO clusters.

A comparison of TPR-1 and TPR-2 peak areas revealed slightly lower H_2 consumption during the second TPR process (about 1.3, 3.5 and 2.5% for CuCe10, CuCe15 and CuCe20 samples, respectively). Again, these changes were more considerable for materials with a higher CuO content and can be tentatively attributed to slightly lower extent of partial CeO_2 reduction.

4. 2. 4. Selective N_2O Chemisorption

CuO dispersion of tested samples was evaluated by selective N_2O chemisorption, carried out at 90 °C, which selectively oxidizes Cu to Cu_2O, without interaction with the CeO_2 support.[32] By adopting the oxidation reaction stoichiometry[33] and equation proposed,[34] the average size of CuO clusters on the surface was calculated. This calculation further assumed that particles are spherical in shape and that only oxidation of Cu monolayer took place. The obtained results are presented in Table 2. The calculated CuO particle size was found to be 1.3, 1.9 and 1.7 nm for CuCe10, CuCe15 and CuCe20 samples, respectively, which corresponds to CuO dispersion being in the range of 28 to 40%. The small size of CuO particles explains the absence of CuO peaks in XRD diffractograms (Figure 5). It is interesting to note that increasing CuO content in Cu-Ce solids does not lead to the formation of larger CuO particles, which was observed in our previous study investigating powdered CuO–CeO_2 catalysts prepared by the method of co-precipitation.[27] Even more, increasing calcination temperature does not significantly influence the CuO particle size, since the calculated average size of Cu-O clusters on the surface of CuCe15 samples (calcined at 400 °C) was larger than the one calculated for CuCe20 sample (calcined at 450 °C). The hard template synthesis method utilized to prepare tested mixed oxides results in BET surface area in excess of 147 m^2/g, which is able to accommodate substantial CuO loadings with surprisingly high CuO dispersion (Table 2).

4. 2. 5. Surface Acidity

Practical applications of finely dispersed metal oxides with pronounced surface area play a fundamental role in numerous adsorptive functions and surface catalyzed reactions. Surfaces of such dispersed oxide materials are expected to be highly irregular and defective, and their properties may be dominated by some particularly energetic and reactive minority defect sites. Such sites can be represented by uncoordinated metal ions or metal clusters, exposed oxide (O^{2-}) ions which are, if not thermally treated, terminated by –OH groups originating from dissociative H_2O adsorption. All these sites express either Lewis or Brønsted acidity. In order to comprehend the mechanism of their catalytic action and predict their activity and selectivity, information on the nature, amount and strength of acid sites exposed on the metal oxide surfaces is needed. NH_3 reacts with both Lewis and Brønsted acid sites, as it can bond to the exposed surface metal cations through the free electron pair of the nitrogen atom, or to Brønsted acid sites by forming a hydrogen bond with the

surface hydroxyl groups. Consequently, NH_3 consumption accounts for titration of all acid sites, capable of reacting with NH_3. Acid site strength was in our experiments evaluated by means of NH_3 temperature programmed desorption. In the previous work,[27] we successfully correlated enhanced surface acidity of powdered CuO–CeO_2 mixed metal oxide catalysts and superior activity of these solids in WGS reaction, thus showing that it is a very important factor contributing to the overall activity in this process.

Results of surface acidity probing of various CuCe mixed oxides are depicted in Figure 12. Besides NH_3 desorption, considerable amounts of CO_2 desorbed from the surface were also detected. It should be noted that CO_2 originates from the process of oxide reduction with diluted CO, as it binds to the catalyst surface forming different carbonate species.[35] At elevated temperatures carbonates decompose and desorb as CO_2. The amount of the latter increases with rising partial CeO_2 reduction and CuO loading (Table 2).

A bimodal NH_3-TPD curve was recorded for all tested samples. The largest amount of NH_3 desorbed, measured over the entire temperature range, was observed for CuCe10 sample (1.24 μmol/m^2), indicating the highest abundance of surface acid sites present in this sample. Lower, but very similar quantities (0.89 and 0.92 μmol/m^2) of NH_3 were desorbed from samples with 15 and 20 mol % CuO.

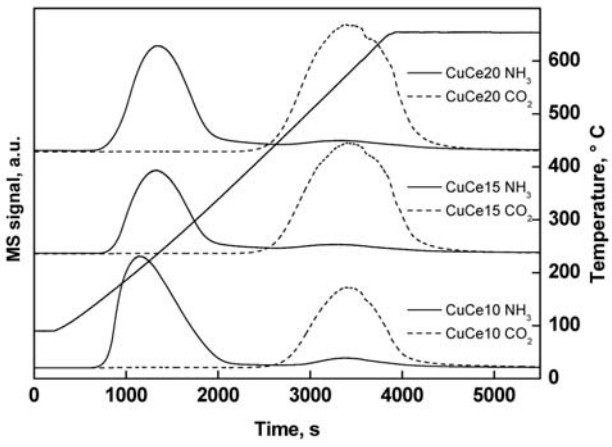

Figure 12. NH_3 and CO_2 desorption from CuCe10, CuCe15 and CuCe20 samples as a function of temperature.

The temperature range of NH_3 desorption (symmetrical peak between 140 and 430 °C with a maximum at around 240 °C) did not differ much for CuCe15 and CuCe20 materials, indicating very similar acid strength distribution in these two samples. In addition, a high temperature NH_3 desorption peak was detected at temperatures between 450 and 650 °C, whose amount was evaluated at 7.2 (CuCe15) and 6.2% (CuCe20) of total NH_3 consumption. On the other hand, CuCe10 sample exhibited a large asymmetric NH_3 desorption peak between 135 and 440 °C with a maximum at 210 °C, and another small peak (accounting for roughly 6% of total NH_3 consumption) between 480 and 650 °C with a maximum at 570 °C. The lower temperature peak exhibited a steep initial rise and pronounced tailing. Asymmetry of this peak indicates noticeable inhomogeneity of acid site strength with emphasis on weak acidic sites, which is probably connected to specific morphology of the CuCe10 sample. For illustration, it should be pointed out that only weak and less abundant acidic sites (NH_3 desorption occurred in the temperature range of 100 to 220 °C) were present on the surface of powdered CuCe catalysts prepared by the co-precipitation technique.[36]

5. Conclusions

Hard template synthesis method using KIT-6 silica as a template proved successful for the preparation of ordered nanocrystalline CuO–CeO_2 mixed oxides with 10, 15, 20 mol % CuO. The synthesized solids calcined in the temperature range from 400 to 550 °C exhibit specific surface area in excess of 147 m^2/g, high pore volume and narrow pore size distribution. With the use of XRD and selective N_2O chemisorption methods, we confirmed the presence of ordered mesoporous FCC CeO_2 with *Ia3d* structural symmetry, average CeO_2 (111) crystallite size of 6.5 nm and CuO dispersion between 28 and 40%, which decreases with increasing CuO loading. The calculated average CuO cluster size was between 1.3 and 1.9 nm with surprisingly low dependence on calcination temperature and CuO content, indicating that the high surface area of CuO–CeO_2 materials can accommodate high loadings of finely dispersed metal clusters. The synthesized materials exhibit remarkable redox properties at low temperatures, with synergistic effect of CuO content on enhanced CeO_2 reduction. H_2-TPR/TPO/TPR cycling caused little change in pore size/volume and specific surface area of tested solids, demonstrating good thermal stability of the CeO_2 skeletal structure under reductive and oxidative conditions, but initiated the migration of CuO clusters on the CeO_2 surface. The employed preparation technique results in abundance of acidic sites on the surface of investigated mixed oxides. The performance of synthesized CuO–CeO_2 materials will be examined in the near future in various solid catalyzed reactions.

6. Acknowledgements

The authors gratefully acknowledge the financial support of the Ministry of Education, Science and Technology of the Republic of Slovenia through Research program No. P2-0152.

7. References

1. W. Liu, M. Flytzani-Stephanopoulos, *J. Catal.* **2005**, *153*, 304–316.
2. L. Kundakovic, M. Flytzani-Stephanopoulos, *J. Catal*. **1998**, *179*, 203–221.
3. A. Tschöpe, W. Liu, M. Flytzani-Stephanopoulos, J. Y. Ying, *J. Catal*. **1995**, *157*, 42–50.
4. W. Liu, A. F. Sarofim, M. Flytzani-Stephanopoulos, *Appl. Catal. B* **1994**, *4*, 167–186.
5. T. Zhu, L. Kundakovic, A. Dreher, M. Flytzani-Stephanopoulos, *Catal. Today* **1999**, *50*, 381–397.
6. M. Fernández-García, E. Gómez Rebollo, A. Guerrero Ruiz, J. C. Conesa, J. Soria, *J. Catal*. **1997**, *172*, 146–159.
7. P. Bera, S. T. Aruna, K. C. Patil, M. S. Hegde, *J. Catal*. **1999**, *186*, 36–44.
8. S. Hočevar, J. Batista, J. Levec, *J. Catal*. **1999**, *184*, 39–48.
9. S. Hočevar, U. Opara Krašovec, B. Orel, A. S. Aricó, H. Kim, *Appl. Catal. B* **2000**, *28*, 113–125.
10. G. Avgouropoulos, T. Ioannides, C. Papadopoulou, J. Batista, S. Hočevar, H. K. Matralis, *Catal. Today* **2002**, *75*, 157–167.
11. G. Sedmak, S. Hočevar, J. Levec, *J. Catal*. **2003**, *213*, 135–150.
12. G. Avgouropoulos, T. Ioannides, *Appl. Catal*. **2003**, *244*, 155–167.
13. Y. Li, Q. Fu, M. Flytzani-Stephanopoulos, *Appl. Catal. B* **2000**, *27*, 179–191.
14. H. Kušar, S. Hočevar, J. Levec, *Appl. Catal. B* **2006**, *63*, 194–200.
15. T. Tabakova, F. Boccuzzi, M. Manzoli, J. W. Sobczak, V. Idakiev, D. Andreeva, *Appl. Catal. A* **2006**, *298*, 127–143.
16. A. Martínez-Arias, M. Fernández-García, J. Soria, J. C. Conesa, *J. Catal* **1999**, *182*, 367–377.
17. M. Fernández-García, A. Martínez-Arias, A. Iglesias-Juez, C. Belver, A. B. Hungría, J. C. Conesa, J. Soria, *J. Catal* **2000**, *194*, 385–392.
18. A. Martínez-Arias, A. B. Hungría, G. Munuera, D. Gamarra, *Appl. Catal. B* **2006**, *65*, 207–216.
19. W. Shen, X. Doug, Y. Zhu, H. Chen, J. Shi, *Microporous Mesoporous Mater*. **2005**, *85*, 157–162.
20. S. C. Laha, R. Ryoo, *Chem. Commun*. **2003**, 2138–2139.
21. A. Rumplecker, F. Kleitz, E.-L. Salabas, F. Schüth, *Chem. Mater*. **2007**, *19*, 485–496.
22. J. Zhu, Q. Gao, Z. Chen, *Appl. Catal. B* **2008**, *81*, 236–243.
23. F. Kleitz, T.-W. Kim, R. Ryoo, *Bull. Korean Chem. Soc*. **2005**, *26*, 1653–1667.
24. E. Rossinyol, J. Arbiol, F. Peiró, A. Cornet, J. R. Morante, B. Tian, T. Bo, D. Zhao, *Sens. Actuators B* **2005**, *109*, 57–63.
25. M. Choi, W. Heo, F. Kleitz, R. Ryoo, *Chem. Commun*. **2003**, 1340–1341.
26. T.-W. Kim, F. Kleitz, B. Paul, R. Ryoo, *J. Am. Chem. Soc*. **2005**, *127*, 7601–7610.
27. P. Djinović, J. Batista, A. Pintar, *Appl. Catal. A* **2008**, *347*, 23–33.
28. A. Martínez-Arias, D. Gamarra, M. Fernández-García, X. Q. Wang, J. C. Hanson, J. A. Rodriguez, *J. Catal*. **2006**, *240*, 1–7.
29. K. Jiao, B. Zhang, B. Yue, Y. Ren, S. Liu, S. Yan, C. Dickinson, W. Zhou, H. He, *Chem. Commun*. **2005**, 5618–5620.
30. A. Pintar, J. Batista, S. Hočevar, *J. Colloid Interface Sci*. **2007**, *307*, 145–157.
31. T. Caputo, L. Lisi, R. Pirone, G. Russo, *Appl. Catal. A* **2008**, *348*, 42–53.
32. J. R. Jensen, T. Johannessen, H. Livbjerg, *Appl. Cat. A* **2004**, *266*, 117–122.
33. M. H. Kim, J. R. Ebner, R. M. Friedman, M. A. Vannice, *J. Catal*. **2002**, *208*, 381–392.
34. J. Kugai, V. Subramani, C. Song, M. H. Engelhard, Y.-H. Chin, *J. Catal*. **2006**, *238*, 430–440.
35. D. Gamarra, G. Munuera, A. B. Hungría, M. Fernández-García, J. C. Conesa, P. A. Midgley, X. Q. Wang, J. C. Hanson, J. A. Rodríguez, A. Martínez-Arias, *J. Phys. Chem. C* **2007**, *111*, 11026–11038.
36. P. Djinović, J. Levec, A. Pintar, *Catal. Today* **2008**, *138*, 222–227.

Povzetek

V prispevku je opisana sinteza $CuO–CeO_2$ mešanih kovinskih oksidov z 10, 15 in 20 mol % CuO po metodi trdne šablone. Za šablono smo uporabili mezoporozni silicijev dioksid – KIT-6. Rezultati XRD analize in N_2 adsorpcijsko/desorpcijskih meritev so potrdili, da imajo sintetizirani materiali urejeno mezoporozno strukturo, ki je inverzna strukturi KIT-6 šablone. Lastnosti $CuO–CeO_2$ oksidov smo preučevali tudi s temperaturno-programiranima tehnikama (H_2-TPR/TPD, H_2-TPR/TPO/TPR), selektivno N_2O kemisorpcijo in s sklopljeno NH_3 kemisorpcijo/TPD analizo. BET specifična površina vzorcev (147–166 m^2/g) je odvisna od vsebnosti CuO in temperature kalcinacije. Disperzija CuO faze se je v sintetiziranih materialih gibala med 28 in 40%, izračunana velikost CuO delcev pa med 1.3 in 1.9 nm. H_2/TPR-TPO-TPR testi kažejo na zanemarljive razlike v spremembah velikosti in volumna por kalciniranih oksidov, kar potrjuje dobro termično stabilnost CeO_2 strukture v reduktivno/oksidativni atmosferi pri povišani temperaturi. Pri teh poskusih smo opazili migracijo CuO delcev na površini CeO_2, kar je močno vplivalo na redoks lastnosti preiskovanih materialov. Strukturno urejeni in porozni $CuO–CeO_2$ oksidi izkazujejo visoko termično obstojnost, dobre redoks lastnosti ter visoko kislost površine, zaradi česar je uporabljena sintezna metoda s trdno šablono zelo primerna za pripravo urejenih, mezoporoznih mešanih kovinskih oksidov kot potencialnih katalizatorjev za heterogeno katalizirane procese.